Toward a novel laser-based approach for validating snow interception estimates

Micah Russell[1], Jan Eitel[1], Andrew Maguire[1], and Timothy Link[1]

[1]University of Idaho College of Natural Resources

April 28, 2020

Abstract

Forests reduce snow accumulation on the ground through canopy interception and subsequent evaporative losses. To understand snow interception and associated hydrological processes, studies have typically relied on resource-intensive point scale measurements derived from weighed trees or indirect measurements that compared snow accumulation between forested sites and nearby clearings. Weighed trees are limited to small or medium sized trees and indirect comparisons can be confounded by wind redistribution of snow, branch unloading, and clearing size. A potential alternative method could use terrestrial lidar (light detection and ranging) because three-dimensional lidar point clouds can be generated for any size tree and can be utilized to calculate volume of the intercepted snow. The primary objective of this study was to provide a feasibility assessment for estimating snow interception mass with terrestrial laser scanning (TLS), providing information on challenges and opportunities for future research. During the winters of 2017 and 2018, intercepted snow masses were continuously measured for two model trees suspended from load-cells. Simultaneously, autonomous terrestrial lidar scanning (ATLS) was used to develop volumetric estimates of intercepted snow. Multiplying ATLS volume estimates by snow density estimates (derived from empirical models based on air temperature) enabled comparison of predicted vs. measured snow mass. Results indicate agreement between predicted and measured values (R2 [?] 0.69, RMSE [?] 0.91 kg, slope [?] 0.97, intercept [?] -1.39) when multiplying TLS snow interception volume with a constant snow density estimate. These results suggest that TLS might be a viable alternative to traditional approaches for mapping snow interception, potentially useful for estimating snow loads on large trees, collecting data from hazardous or remote terrain, and calibrating snow interception models to new forest types around the globe.

1. Introduction

The hydrology of snow dominated forests is controlled by interactions of mass and energy fluxes between snow and forest structural elements. As forest cover increases, snow accumulation on the ground is typically reduced because of canopy snowfall interception and subsequent sublimation, which can account for as much as 60% of the cumulative snowfall depending on forest type, duration of snow storage in the canopy, and seasonal hydrometeorological conditions (Hedstrom & Pomeroy 1998; Molotch et al., 2007). The sensitive connection between forest structure and snow interception therefore has important implications for the hydrology in any region around the globe where the major proportion of total water input comes from snow. Understanding this relationship is increasingly important with widespread observed and projected shifts from snow to rain (Klos et al., 2014), changes in the frequency of winter rain-on-snow events (Floyd & Weiler, 2008; Musselman et al., 2018), and changes in forest vegetation due to fire (Westerling, 2016), drought (Allen et al., 2010), insects (Bentz et al., 2010; Frank, Massman, Ewers, & Williams, 2019) and other disturbance processes that might be altered by a changing climate and/or forest management.

While the importance of snow interception has long been acknowledged, it is also difficult to measure, map, and model. Direct measurement has typically been limited to resource-intensive point measurements derived from weighed trees, which are generally limited to small or medium trees (Hedstrom & Pomeroy, 1998; Knowles, Dettinger, & Cayan, 2006; Storck et al., 2002; Suzuki & Nakai, 2008) or tree branches (Brundl,

Bartelt, Schneebeli, & Fluhler, 1999; Schmidt & Gluns, 1991). Indirect measurements have compared snow accumulation between forested sites and nearby clearings. Although indirect measurements have advantages (e.g. estimating spatial variance), the accuracy has long been questioned (e.g., Miller 1964) and the measurements can be confounded by wind redistribution of snow, branch unloading, and reference site size (Moeser, Stähli, & Jonas, 2015).

A potential novel method could use terrestrial lidar (TLS) because three-dimensional lidar point clouds, based on the laser return-time/distance relationship, can be generated for any size tree. The point clouds can be transformed into an α-shape (convex hull with a polyhedral surface approximating the shape and volume the tree), from which volumes can be calculated (Edelsbrunner, 1994; Lafarge, Pateiro-Lopez, Possol & Dunkers, 2014). The α-shape convexity (i.e. α-convexity) (Rodriguez-Casal, 2007) is tunable according to TLS spatial resolution and study objectives – be it calculating volumes of fine-scale structures like branches or smoothed-over structures like snow-laden trees. Intercepted snow volume can be estimated by subtracting snow-free tree volume from snow-on tree volume. Furthermore, novel autonomous terrestrial laser scanning (ATLS) systems (Adams et al., 2014; Eitel et al., 2013) could enable timeseries characterization of seasonal dynamics associated with snow interception and unloading. Ultimately, TLS based snow interception may have a number of advantages over traditional methods, including: spatially explicit estimation of snow interception for different aspects or portions of tree canopies, data collection in difficult to access terrain (Adams, Bauer, & Paar, 2014) known to be important contributors to water budgets (Bühler, Adams, Bösch, & Stoffel, 2016; Hood & Hayashi, 2010), and providing time-efficient data for calibration of emerging aerial lidar (ALS)-based snow interception models to specific forest types (Deems et al., 2013; Moeser et al., 2015; Painter et al., 2016).

The objectives of this study were twofold: (1) Test the feasibility of using ATLS to directly map intercepted snow mass and (2) Determine the effect of α-convexity on ATLS-derived snow mass estimates. In doing so, this study provides a preliminary feasibility assessment for estimating snow interception mass with terrestrial laser scanning, providing information on challenges and opportunities for future research.

2. Methods

2.1 Study Site

Two model hanging trees measuring 1.83 meters (m) in height (hereafter referred to "left tree" and "right tree" - see Figure 1) were installed prior to winter 2017 following established approaches outlined in Hedstrom and Pomeroy, 1998. The trees were off-the-shelf Christmas trees, bilaterally symmetrical and not representing a specific species. Artificial trees were utilized to avoid desiccation and interception estimates that may be affected by progressive needle drop. The trees were installed at the University of Idaho McCall Field Campus (44.9353472°, -116.0820167°) in the mountains of west-central Idaho, which receives an average of 3.4 m of snow fall (depth) per year at 1528 m elevation (Western Regional Climate Center, 2016).

2.2 Field Measurements

Load cells measured strain gauge output (mV/V), an electrical signal which is proportional to the applied excitation voltage, from the hanging trees in one-minute intervals. Known masses were hung from the load cells to verify measurement accuracy and to develop a calibration equation (mass = 30.18 * mV/V – 4.6917) which converted strain gauge output to kg. The originating mass of a snow-free tree at the beginning of each winter was subtracted from subsequent measurements to calculate snow masses for each scan.

An ATLS scanned one side of the trees at a distance of 6.2 m and produced two high resolution point clouds per day (1.12 cm spot size and 0.20 cm point spacing at 10 m) (Figure 1b). The ATLS employs a rugged time-of-flight laser rangefinder (optoNCDT ILR 1191 with 905 nm near infrared laser and 1.7 mrad beam divergence; Micro-Epsilon Messtechnik GmbH & Co. KG, Ortenburg, Germany) designed for harsh environments (see Eitel et al., 2013 for more detail). The ATLS completed one scan in 13 hours.

Assuming each tree canopy to be bilaterally symmetrical and circular in shape, and given a known canopy diameter, distance from scanner to canopy perimeter, and location of the ATLS, trigonometric calculations

yielded 47.7% for the percent of tree canopy perimeter "seen" by the ATLS. Rounded to 50% for the analyses, snow masses obtained from the load cells were therefore divided by two and averaged across each ATLS scan duration to allow for comparison with ATLS data.

2.3 Lidar volume estimates

The ATLS point clouds were transformed into "alpha-shape" structures in R using the alphashape3d R package (Lafarge, Pateiro-Lopez, Possol and Dunkers, 2014). An alpha-shape structure is a three-dimensional convex hull generated from a point cloud, approximating the shape and volume of the scanned structure. The convex hull is fitted with Delauney Triangulation (drawing triangles between points so that there is no overlap between triangles). The α-convexity parameter (α) (Edelsbrunner & Mucke, 1994) is selected by the user, corresponding to data resolution and units of the input data. An α-convexity parameter of 1 corresponds to the convex hull; the closer α is to zero, the more triangle borders are deleted to make a better fitting, flexible and concave hull (see Figure 3). A sensitivity analysis was conducted by comparing measured vs. ATLS derived snow mass (see section 2.5) with α = 0.010, 0.015, 0.020, 0.025, and 0.030 m – a range deemed appropriate given the ATLS spatial resolution (see section 2.2). This permitted the selection of α that resulted in the best agreement between observed and TLS based estimates of intercepted snow mass. The originating volume of a snow-free tree at the beginning of each winter was subtracted from subsequent measurements to calculate snow volumes for each scan.

2.4 Snow density estimates

Fresh snow density (kg/m3) was estimated using hourly air temperatures (??; 0.1° C resolution) from a meteorological monitoring sensor equipped with a radiation shield (VP-4, METER, Pullman, WA) positioned on a pole directly above the ATLS. Several methods of estimating fresh snow density from air temperature were tested, including:

ρ (Brazenec) = constant density of kg/m3 estimated for the Rocky Mts. [1] (Brazenec, 2005)

ρ (Diamond-Lowry) = 119 + (6.48*??) [2] (Diamond & Lowry, 1953)

ρ (LaChapelle) =) 50 +1.7(Ta +15)1.5[3] (LaChapelle, 1962)

ρ (Hedstrom-Pomeroy) = 67.92+51.25?(??/2.59) [4] (Hedstrom & Pomeroy, 1998)

Mean fresh snow density was calculated for each ATLS scan time interval (13 hours). Estimates of snow interception were calculated by multiplying the laser derived snow volumes (m3) with fresh snow densities derived from equations [1-4] (kg m-3).

2.5 Statistical analysis

The precision and accuracy of laser derived estimates of snow interception (objective 1) was determined by fitting a simple linear regression model in R (R Core Team, 2013) between ATLS derived intercepted snow mass in kg (independent variable) and load cell derived intercepted snow mass in kg (dependent variable) (Piñeiro, Perelman, Guerschman, & Paruelo, 2008). Following common practice when using convex hull approaches (e.g., Lafarge, Pateiro-Lopez, Possol & Dunkers, 2014), a sensitivity analysis to determine the effect of α-convexity on ATLS derived snow mass estimates (objective 2) was performed by comparing R2 (goodness-of-fit), Root Mean Square Error (RMSE) in kg, and regression intercept/slope estimates (indicative of model bias) for each model combining alternative α levels (see section 2.3) and snow density estimation methods (see section 2.4). The optimal model was determined by selecting, first, the best performing snow density estimation method and, secondly, the α level that produced the least under/over estimation in ATLS based mass predictions (i.e. closest to 1:1 line) and lowest RMSE.

3. Results

A total of 115 complete ATLS scans were recorded for the left tree in the first winter between January and April; a total of 69 complete ATLS scans were recorded for the left tree in the second winter between November and March. A total of 83 and 69 scans were recorded for the right tree over the same time periods.

Discrepancies in sample size between the left and right tree were related to incomplete ATLS scans in which scanner malfunction truncated a portion of the scene(e.g., see Figure 1b).

Data exploration using results from the left tree revealed that measured snow interception (averaged across multiple complete scans) in the first winter averaged 3.19 kg (1.0% of season total), with a standard deviation of 4.59 kg and a maximum of 16.95 kg (4.8% of season total). During the second winter, measured snow interception for the left tree averaged 3.31 kg (2.3% of season total), with a standard deviation of 2.76 kg and a maximum of 10.19 kg (4.5% of season total). Estimated mean fresh snow densities using equations [1-4] for the left tree in both winters are summarized in Table 1. Density values are similar to Mair et al. (2016), in which estimates produced by equation [2] approximated the Brazenec (2005) constant, estimates produced by equation [3] were higher than the constant, and estimates produced by equation [4] displayed a wider range.

Sensitivity analyses (Table 2) using data spanning both winters for both trees demonstrated that the fresh snow density constant [1] (Brazenec, 2005) consistently produced higher R2 (model fit) and lower RMSE (unexplained variance) than empirical variable-density equations [2] (Diamond & Lowry,1953), [3] (LaChapelle, 1962), and [4] (Hedstrom & Pomeroy), in that order. An α-convexity parameter of $\alpha = 0.025$ was selected for further analysis because, at this level, regressions utilizing the density constant produced slopes close to 1.00 (0.97 for the left tree and 1.07 for the right tree), calibrating the two methods (see Figure 2). Underestimation in TLS based mass estimates is evident with $\alpha = 0.010$, 0.015, and 0.020 m; overestimation in TLS based mass estimates is evident with $\alpha = 0.025$ and $\alpha = 0.030$ m (see slopes in Table 2). Simple linear regression utilizing the density constant and α-shape resolution of 0.025 m yielded R2 = 0.71 / RMSE = 1.06 kg for the left tree and R2 = 0.69 / RMSE = 0.91 kg for the right tree. Intercepts of -1.39 for the left tree and -1.34 for the right tree further illustrate model bias.

4. Discussion

4.1 The effect of snow density and scan duration on model performance

To our knowledge, this is the first study that explores the suitability of high resolution, automated terrestrial lidar to directly estimate canopy snow interception, with direct comparison to the established hanging tree method (Hedstrom & Pomeroy, 1998). The most precise proxies for measured snow interception mass (R2 [?] 0.69), with the least variation in unexplained variance (RMSE [?] 0.91 kg), were obtained by multiplying the ATLS-derived snow interception volume estimates by a regionally specific fresh snow density constant or 100 kg/m3 (Brazenec, 2005). A density constant of 120-125 kg/m3, a reasonable estimation for the region, would have further improved model performance.

In contrast, ATLS-derived snow interception volume estimates in conjunction with dynamic fresh snow density estimation equations based on air temperature reduced R2 and increased RMSE model estimates. It may be that because equations [2-4] are empirical, they represent relationships between fresh snow density and air temperature specific to their respective experimental locales: Sierra Nevada Mountains in California (Diamond & Lowry, 1953); mid-continental Canadian boreal forest (Hedstrom & Pomeroy, 1998); and, a variety of avalanche monitoring sites across the western United States (LaChapelle, 1962). Unexplained model variance in ATLS based mass predictions may also be partially explained by the long ATLS scan duration (13 hours). subsequent changes to the density of freshly intercepted snow (i.e. metamorphosis) during the course of one scan, or retention of metamorphosed snow between snow events, may have resulted in unexplained model variance. Furthermore, this study was not designed to account for losses of intercepted snow due to wind-driven sublimation and/or unloading, processes that also may have resulted in unexplained model variance.

The exclusive reliance on fresh snow density equations that don't take snow metamorphosis into account (Brazenec, 2005; Diamond & Lowry, 1953; Hedstrom & Pomeroy, 1998; LaChapelle 1962) likely contributed to model noise and/or underestimation of predicted density/mass, and experimental development of adjustment factors for these equations was not in the scope of this study. Although under- and overestimation were minimized by conducting a sensitivity analysis to select the degree of α-convexity (see section 4.3), these

conclusions point to the need for shorter ATLS scan durations. Recent advances in lidar technology might help to address the slow scan duration time with the relatively new availability of rugged, relatively low-cost (< $10,000), fast scanning lidar instruments (Condliffe, 2018). Further, laser return intensity obtainable from TLS might provide valuable insights on snow properties that affect density, such as changes in grain size/shape and overall wetness (e.g., Eitel et al., 2016, Kaasalainen, Kaartinen, & Kukko, 2008). Although this study emphasized automated data collection, model performance could also have been improved with *in situ* density measurements of intercepted snow. Further research is of sampling snow density on trees.

4.2 The effect of weather and snow properties on model performance

TLS can detect minute changes (<10cm) in snow depth, but several factors can decrease the number and intensity of received signals (Deems, 2013; Prokop, 2008). Atmospheric occlusion from heavy snow or fog can interfere with lidar returns, and wet snow surfaces can lead to adsorption of lidar pulses on the target itself (Deems, 2013; Kaasalainen, Kaartinen, & Kukko, 2008; Prokop, 2008). Snow is also strongly forward-scattering; the proportion of forward scattering of lidar pulses increases with scan angle (Deems, 2013), potentially leading to missed returns on the edges of targets. Despite these issues, the short distance to target (6.2 m) and small scan angle (4.22°) should have minimized the variance between measured and ATLS derived snow mass due to atmospheric occlusion or forward scattering. Likewise, sampling during the coldest months should have minimized unexplained model variance or underestimation of snow volume due to lidar pulse adsorption by snow with high water content. Although these confounding factors were minimized, they were not entirely eliminated in this pilot study.

5. Conclusion

This study provides valuable insights into the use of TLS for estimating snow interception mass with terrestrial lidar data. Initial results indicate agreement between predicted and measured values of intercepted snow mass (R2 [?] 0.69 and RMSE [?] 0.91 kg) when utilizing an α-shape convexity parameter (α) of 0.025 m and a constant snow density estimate (100 kg/m3). To further improve TLS derived snow interception estimates, future research is needed to develop improved approaches to estimate *in situ* canopy intercepted snow density, explore the sensitivity of TLS snow volume estimates to changing snow conditions and quantities within the canopies of a variety of live trees of different sizes and for a range of temperatures that affect branch flexibility, and/or reduce beam divergence and reconstruct occluded structural elements. Snow interception is challenging to measure or model, but our findings highlight the potential of lidar technology to efficiently and accurately estimate intercepted snow mass. This is a potentially useful development for the collection of interception data in remote terrain, as well as the calibration of aerial lidar-based snow interception models to distinct forest types around the globe.

6. Acknowledgements

Micah Russell was supported by National Aeronautics and Space Administration Earth & Space Science Fellowship Program (18-EARTH18F-0208), National Science Foundation Integrative Graduate Education and Research Traineeship Program, and the Curt Berklund Graduate Research Scholar Fund. Jan Eitel and Andrew Maguire were supported by the NASA ABoVE grant NNX15AT86A. Jan Eitel was further supported by the National Institute of Food and Agriculture, U.S. Department of Agriculture, McIntire Stennis project under 1018044.

7. Data Availability Statement

The data that support the findings of this study are available from the corresponding author upon reasonable request.

8. References

Adams, M S, Bauer A, & Paar G. 2014. Monitoring snow avalanche terrain with automated terrestrial laser scanning. *Geoscience and Remote Sensing Symposium 2014* , 4006-4009.

Allen, C D, Macalady, A K, Chenchouni, H, Bachelet, D, McDowell, N, Vennetier, M, ... & Cobb, N. 2010. A global overview of drought and heat-induced tree mortality reveals emerging climate change risks for forests. *Forest Ecology and Management* , *259* (4), 660-684.

Bentz, B J, Régnière, J, Fettig, C J, Hansen, E M, Hayes, J L, Hicke, J A, ... & Seybold, S. J. 2010. Climate change and bark beetles of the western United States and Canada: direct and indirect effects. *BioScience* , *60* (8), 602-613.

Brazenec W A. 2005. *Evaluation of ultrasonic snow depth sensors for automated surface observing systems (ASOS)* (PhD Thesis). Colorado State University Fort Collins, Colorado.

Brundl M, Bartelt P, Schneebeli M, & Fluhler H. 1999. Measuring branch defection of spruce branches caused by intercepted snow load.*Hydrological Processes* , *13* (14–15), 2357–2369.

Condliffe, J. 2018. This new lidar sensor could equip every autonomous car in the world by the end of 2018. *MIT Technology Review* . Retrieved from https://www.technologyreview.com/ .

Diamond M, & Lowry W P. 1953. *Correlation of the Density of New Snow with 700 Mb Temperature (Vol. 1)*. Snow, Ice and Permafrost Research Establishment, Corps of Engineers, US Army.

Deems, J S, Painter, T H, & Finnegan, D C. 2013. Lidar measurement of snow depth: a review. *Journal of Glaciology* , *59* (215), 467-479.

Eitel, J U, Vierling, L A, & Magney, T S. 2013. A lightweight, low cost autonomously operating terrestrial laser scanner for quantifying and monitoring ecosystem structural dynamics. *Agricultural and Forest Meteorology* , *180* , 86-96.

Eitel, Jan U H, Höfle, B, Vierling, L A, Abellán, A, Asner, G P, Deems, ... & Vierling, K T. 2016. Beyond 3-D: The new spectrum of lidar applications for earth and ecological sciences. *Remote Sensing of Environment* , *186* (C), 372-392.

Edelsbrunner H, & Mucke E P. 1994. Three-Dimensional Alpha Shapes.*ACM Transactions on Graphics* , *13* (1), 43–72.

Floyd W, & Weiler M. 2008. Measuring snow accumulation and ablation dynamics during rain-on-snow events: innovative measurement techniques.*Hydrological Processes* , *22* (24), 4805–4812.

Frank, J M, Massman, W J, Ewers, B E, & Williams, D G. 2019. Bayesian Analyses of 17 Winters of Water Vapor Fluxes Show Bark Beetles Reduce Sublimation. *Water Resources Research* , *55* (2), 1598-1623.

Hedstrom N R, & Pomeroy J W. 1998. Measurements and modelling of snow interception in the boreal forest. *Hydrological Processes* ,*12* (10-11), 1611–1625.

Hood J, & Hayashi M. 2010. Assessing the application of a laser rangefinder for determining snow depth in inaccessible alpine terrain.*Hydrology and Earth System Sciences* , *14* (6), 901.

Kaasalainen, S, Kaartinen, H, & Kukko, A. 2008. Snow cover change detection with laser scanning range and brightness measurements.*EARSeL eProc* , *7* (2), 133-141.

Klos, P Z, Link, T E, & Abatzoglou, J T. 2014. Extent of the rain-snow transition zone in the western US under historic and projected climate.*Geophysical Research Letters* , *41* (13), 4560-4568.

Knowles, N, Dettinger, M D, & Cayan, D R. 2006. Trends in snowfall versus rainfall in the western United States. *Journal of Climate* ,*19* (18), 4545-4559.

LaChapelle, E R. 1962. *The density distribution of new snow* . Alta Avalanche Study Center.

Lafarge, T, Pateiro-Lopez, B, Possolo, A, & Dunkers, J. 2014. R Implementation of a Polyhedral Approximation to a 3D Set of Points Using the Alpha-Shape. *Journal of Statistical Software* , *56* (1), 1-19.

Mair, E, Leitinger, G, Della Chiesa, S, Niedrist, G, Tappeiner, U, & Bertoldi, G. 2016. A simple method to combine snow height and meteorological observations to estimate winter precipitation at sub-daily resolution. *Hydrological Sciences Journal* ,*61* (11), 2050-2060.

Miller, D H. 1964. Interception processes during snowstorms. *Res. Paper PSW-RP-18* . Berkeley, CA: Pacific Southwest Forest & Range Experiment Station, Forest Service, US Department of Agriculture, 18-43.

Moeser D, Stahli M, & Jonas T. 2015. Improved snow interception modeling using canopy parameters derived from airborne LiDAR data. *Water Resources Research* , *51* (7), 5041–5059.

Molotch, N P, Blanken, P D, Williams, M W, Turnipseed, A A, Monson, R K, & Margulis, S A. 2007. Estimating sublimation of intercepted and sub-canopy snow using eddy covariance systems. *Hydrological Processes: An International Journal* , *21* (12), 1567-1575.

Musselman, K N, Lehner, F, Ikeda, K, Clark, M P, Prein, A F, Liu, C, Barlage, M, & Rasmussen, R. 2018. Projected increases and shifts in rain-on-snow flood risk over western North America. *Nature Climate Change* , *8* (9), 808.

Painter, T H, Berisford, D F, Boardman, J W, Bormann, K J, Deems, J S, Gehrke, F, ... & Winstral, A. 2016. The Airborne Snow Observatory: Fusion of scanning lidar, imaging spectrometer, and physically-based modeling for mapping snow water equivalent and snow albedo. *Remote Sensing of Environment* , *184* , 139-152.

Pineiro, G, Perelman, S, Guerschman, J P, & Paruelo, J M. 2008. How to evaluate models: observed vs. predicted or predicted vs. observed? *Ecological Modelling* , *216* (3-4), 316-322.

Prokop, A. 2008. Assessing the applicability of terrestrial laser scanning for spatial snow depth measurements. *Cold Regions Science and Technology* , *54* (3), 155-163.

R Development Core Team. 2013. *R: A Language and Environment for Statistical Computing.* R Foundation for Statistical Computing, Vienna, Austria.

Russell, M T, Eitel J H, Maguire A J, & Link T E. 2019. Snow interception dataset. Northwest Knowledge Network. DOI t.b.d.

Schmidt R A, & Gluns D R. 1991. Snowfall interception on branches of three conifer species. *Canadian Journal of Forest Research* ,*21* (8), 1262–1269.

Suzuki K, & Nakai Y. 2008. Canopy snow influence on water and energy balances in a coniferous forest plantation in northern Japan. *Journal of Hydrology* , *352* (1), 126–138.

Westerling, A L. 2016. Increasing western US forest wildfire activity: sensitivity to changes in the timing of spring. *Philos Trans R Soc Lond B Biol Sci* , *371* (1696).

Western Regional Climate Center. 2016. Retrieved from https://wrcc.dri.edu/.

Xie, D, Wang, X, Qi, J, Chen, Y, Mu, X, Zhang, W, & Yan, G. 2018. Reconstruction of single tree with leaves based on terrestrial lidar point cloud data. Remote Sensing, *10* (5), 686.

Tables and Figures

Table 1. Mean snow density estimates for the left tree in both winter sampling periods utilizing each density estimation method [1-4] (Brazenec, 2005; Diamond & Lowry, 1953; Hedstrom & Pomeroy, 1998; LaChapelle 1962).

Table 2. Sensitivity analysis with simple linear regression results comparing predicted and measured snow interception mass for each density estimation method [1-4] (Brazenec, 2005; Diamond & Lowry, 1953; Hedstrom & Pomeroy, 1998; LaChapelle 1962) and α-shape convexity parameter (α) (Lafarge et al., 2014). Data spans winters 2017-2018. Equation [1], the snow density constant (Brazenec, 2005), produced the best model

fit and lowest error for both trees. $\alpha = 0.025$ m selected because the regression utilizing the constant produced a slope that most closely approximated a 1:1 line, calibrating the two methods by minimizing over/under estimation in the TLS based estimates.

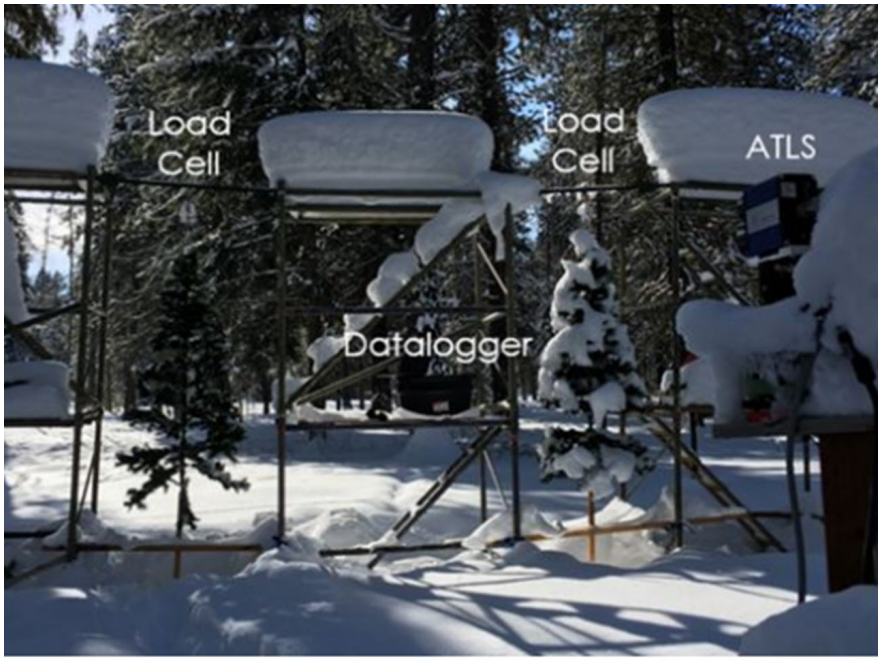

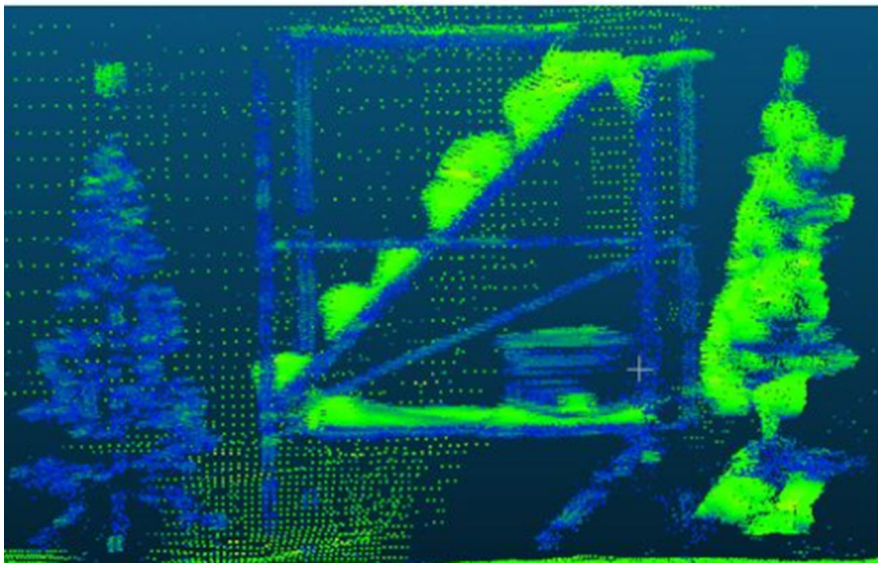

Left tree: ρ(Brazenec)[1]

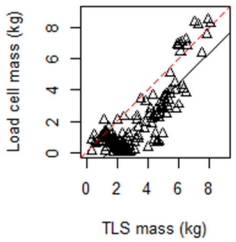

Left tree: ρ(Diamond-Lowry)[2]

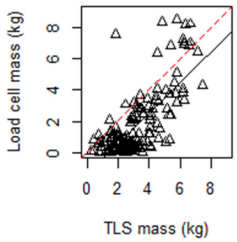

Left tree: ρ(LaChapelle)[3]

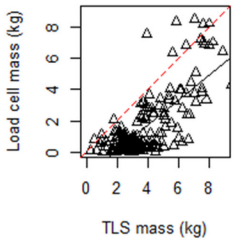

Left tree: ρ(Hedstrom-Pomeroy)[4]

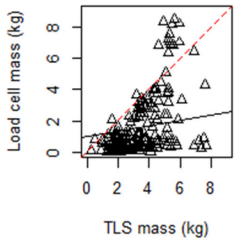

Right tree: ρ(Brazenec)[1]

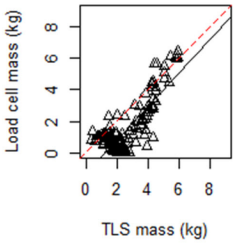

Right tree: ρ(Diamond-Lowry)[2]

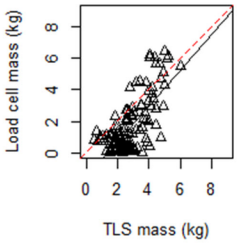

Right tree: ρ(LaChapelle)[3]

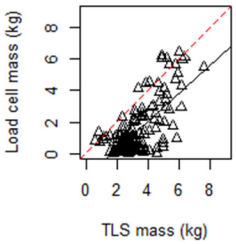

Right tree: ρ(Hedstrom-Pomeroy)[4]